November 17, 1995 Final Report II

Measurement of the Surface Properties of High Temperature Oxides

by

Aiguo Feng, Benjamin J. McCoy, Zuhair A. Munir

Department of Chemical Engineering and Materials Science

University of California, Davis, CA 95616

zamunir@ucdavis.edu

916-752-0592 FAX 916-752-8240

and

Domenick Cagliostro

Thermal Protection Branch

NASA Ames Research Center

Moffett Field, CA 94035

Final Report II for

NASA-Ames University Consortium (No. 5090)

Table of Contents

1. BACKGROUND

The current waterproofing method applied to the space shuttle tiles uses silane agents such as dimethylethoxysilane (DMES) to react with the surface hydroxyl groups (OH) on the silica fiber insulation material[1,2]. This reaction results in the replacement of surface OH groups by methylsilane functional groups, such as O-Si$(CH_3)_2$H. This approach is time and labor intensive and poses environmental hazards. However, the major shortcoming of such a waterproofing method is its limited effectiveness: it provides protection for only one flight or one high temperature thermal cycle. Thus, it is considered a temporary waterproofing method. It remains as a goal to develop a new method that will render the silica surfaces hydrophobic for many thermal cycles.

1.1 Capillary Action

Due to their porous structure, silica insulation tiles[3] absorb water through capillary action. Figure 1 illustrates the water absorption phenomenon on silica tiles. Suppose the contact angle of water on silica surfaces is θ, and its relation with surface tension of water σ_w , surface tension of silica σ_s, and interface tension σ_{ws} follows Young's equation,[4,5] i.e.

$$\sigma_s - \sigma_{ws} - \sigma_w \cos\theta = 0$$
$$or \quad \cos\theta = \frac{\sigma_s - \sigma_{ws}}{\sigma_w} \tag{1.1}$$

For a silica surface, θ is less than 90° because σ_{ws} is less than σ_s.

As a column of water enters into a capillary formed by silica surface as shown in Figure 2(a), there is a pressure difference[4,5] of $2\sigma(1/r_2 - 1/r_1)\cos\theta$ between P_1 and P_2. This difference will be positive if the contact angle θ is less than 90° as is the case for silica. This pressure difference forces the water column to travel further into

the capillary at the location where the radii are the same as shown in Figure 2(b). At that location, the column of water reaches its final equilibrium condition.

Surfaces are classified as non-wetting or hydrophobic if the contact angle of water on them is greater than 90°. Likewise, if $\theta < 90°$, surfaces are classified as wetting or hydrophilic. This classification of wettability is used throughout this report.

1.2 Thermodynamics of Wetting

Thermodynamic considerations can give a fundamental understanding of the contact angle and wetting phenomenon. They also provide the basis for the application of this phenomenon. The work of cohesion, W_c and the work of adhesion $W_{a(1,2)}$ are two fundamental thermodynamic properties. They represent the reversible work required to separate two surfaces of unit area of a material with a surface tension σ, and two materials with surface tensions σ_1 , σ_2 and their interface tension σ_{12}, respectively.[4,5] Thus,

$$W_c = 2\sigma \quad and \quad W_{a(12)} = \sigma_1 + \sigma_2 - \sigma_{12} \tag{1.2}$$

From Equation 1.1, the contact angle can be related to these terms as

$$\cos\theta = -1 + 2\frac{W_{a(sw)}}{W_{c(w)}} \tag{1.3}$$

where $W_{c(w)}$ is the work of cohesion for water, and $W_{a(sw)}$ is the work of adhesion between water and a silica surface. Figure 3 shows the wettability diagram in relation to the values of σ_s and σ_{ws}. As indicated, the competition between $W_{c(w)}$, the tendency of water to adhere to itself, and $W_{a(sw)}$, the attraction between water and the solid surface determines the wettability of water on the surface. It can be concluded that for a non-wetting surface, the relationship

$$W_{c(w)} > 2W_{a(sw)} \tag{1.4}$$

must be valid if the contact angle is larger than 90°.

1.3 Metal Oxide Surfaces

Metal oxides are generally ionic, especially for metals with a low ionization potential and electron affinity[6,7]. The structure, therefore, consists of metal ions surrounded by oxygen ions and vice versa. The various structures of metal oxides can be derived from close packing of MO_x, where M is a metal element and x can vary from 1 to 3. The structures include various types such as rocksalt, MO; corundum, M_2O_3; rutile, MO_2, and so on. Due to their strong ionic bonding and high lattice energies (or Madelung energies), many metal oxides are very stable and resistant to further oxidation at temperatures above 1000 °C, such as TiO_2. The thermal stability of metal oxides is a desirable property for their possible use as water-proof coatings on silica for the thermal protection system (TPS) of the space shuttle.

But there is little experimental and theoretical information available on the wettability of these metal oxides surfaces. It is known from various studies[8,9] that freshly cleaved metal oxide surfaces are highly reactive with water. Water vapor reacts with acidic and basic surface sites through a chemisorption process.
The reaction with water vapor results in the surface hydroxylation, i.e.

$$\left|\begin{matrix}\equiv M \\ \equiv M-O\end{matrix}\right. + H_2O = \left|\begin{matrix}\equiv M-OH \\ \equiv M-OH\end{matrix}\right. \qquad (1.5)$$

The effect of the chemisorption on the wettability of the metal oxide surfaces is two-fold. By the formation of the hydroxyl groups, the surface energy of the oxide can be significantly lowered. On the other hand, the hydroxyl group can form a hydrogen bond with water, thus the surface displays a stronger adhesion to water. The wettability of metal oxide surfaces is also dependent on the surface density, N_s, of hydroxyl groups. The lower the density, the lower is the adhesion interaction between water and the oxide surface. Since the value of N_s varies within a range of 2 to 12 sites per square nanometer[7], we expect the work of adhesion for water on metal oxide surfaces to vary for different surfaces.

2. EXPERIMENTAL METHODS AND MATERIALS

2.1 Surface Preparation

In the present study, metal oxide surface preparation involved oxidation of polished metal surfaces to create a thin oxide layer. For TiO_2, HfO_2, and ZrO_2 preparation, we obtained the respective metal foils from Johnson & Matthey (Alfa) for the first two and Electronic Space Product International (ESPI) for the third. The specifications of the metal foils are listed in Table 1. They were polished according to the steps listed in Table 2. A representative optical micrograph image of a polished Ti metal surface is presented in Figure 4(a). The polished surface was mildly etched by wiping the surface with a cotton swab containing a solution of hydrofluoric acid (HF), nitric acid (HN_3O), and acetic acid (CH_3CO_2H) to remove the surface contaminants due to polishing. The acid solution was made in the approximate proportion of 1:1:1 by volume. The etched Ti surface is shown in Figure 4(b). Prior to the oxidation and contact angle measurements, the polished surfaces were cleaned with acetone to remove residual water.

The oxide layers were formed on polished metal surfaces by oxidation under controlled thermal and gas conditions. Oxidation was carried out inside a quartz tube heated by a resistance heater under a flow of pure gases or room air. The various oxidation conditions employed in this study are listed in Table 3.

2.2 Contact Angle Measurements

For contact angle measurements, we used the sessile-drop method in air. A schematic of the contact angle measurement setup is shown in Figure 5. The drops (about 1~2mm in diameter) are pure distilled water with a surface tension[5] of 72.8 mN/m. The water drop images were captured by a CCD camera behind a Wild Heerbrugg optical microscope and the images were recorded into a PC computer. The contact angle θ was measured directly from the photoimage using the formula

$$\theta = \sin^{-1}\left(\frac{hd}{h^2 + d^2/4}\right) \tag{2.1}$$

where h is the height of the drop and d is its diameter. The measurement error of the contact angle was estimated to be ~1°.

Figure 6 shows the optical micrographs of sessile drops on the Ti metal surfaces (no thermal oxidation) with and without polishing. The contact angle for the polished surface is nearly equal to 90° as shown in Figure 6(a), while the contact angle on the as-received unpolished surface is 55°. The lower value for the unpolished surface can be attributed to the effect of surface roughness as will be discussed below.

Contact angle measurements on oxidized Ti surfaces are illustrated in Figure 7 for different oxidation conditions. It can be seen that the contact angles on all polished and annealed surfaces (Figures 7(a)-7(c)) are the same within the range of experimental uncertainty. However, the contact angle measured immediately after oxidation was remarkably smaller for the Ti surface, as shown in Figure 7(d). Ti surfaces which were not well-polished gave different results. Figure 8 shows a polished Ti foil containing micrometer-sized grooves. The sessile drop images on such a surface (oxidized and unoxidized) are shown in Figure 9. The contact angles on these partially polished surfaces are less than those on well-polished surfaces.

Contact angle measurements on surfaces of Zr and Hf with or without polishing and with or without oxidation were also carried out. Table 4 summarizes the results on various types of metal and metal oxide surfaces.

2.3 Surface Characterization

The metal oxide surfaces were characterized by AES/ESCA. A Perkin Elmer Model 3027 DPCMA ESCA/AES system was used for the analysis. The energy resolution of the spectrometer is about 3.5 eV.

The polished Ti foil sample, treated in oxygen at 300 °C for 10 min was analyzed. The oxidized sample surface contained oxygen, argon, and carbon as well as titanium as indicated in Figure 12. The strong oxygen peak confirmed the presence of the surface oxide layer following thermal treatment. Argon on the surface resulted from Ar ion sputtering for surface conditioning. The ESCA spectrum in Figure 13 reveals the presence of TiO_2 in the surface layer. Figure 13 shows that the Ti (2p3/3) electron binding energy changes as the surface atoms are sputtered away by Ar ions. The (a) spectrum before Ar sputtering reveals two peaks corresponding to Ti metal and Ti bonded to O. This may indicate that oxides on the surface are in island formation. As surface atoms are sputtered away, the spectrum shows a decrease in the 2p3/2 peak corresponding to Ti with oxygen. From the estimated sputtering yield and the decreases of the peaks with time, an oxide layer thickness of ~ 1000 Å can be roughly calculated.

The formation of the oxide surface layer can also be verified by X-ray diffraction analysis of the surfaces. Figure 14 shows the X-ray diffraction measurements on thermally-treated Zr foil. As can be seen from Figure 14, two crystalline structures of ZrO_2 were formed on the surface: the orthorhombic and monoclinic.

3. RESULTS AND DISCUSSION

3.1 Surface Roughness Effect on Contact Angle

Experimental measurements have shown that contact angles depend on whether the sample is polished or not and also on how well it is polished. These

observations indicate that surface roughness plays a role in the equilibrium state of the sessile drop. Previous work has shown a similar dependence[10]. It has been proposed that for rough surfaces, Young's equation can be modified to the following[11,12]:

$$\sigma_w \cos\theta = R_w(\sigma_s - \sigma_{sw}) \qquad (3.1)$$

where R_W is the surface roughness factor, defined as the ratio of the true and apparent surface areas of the surface. If the contact angle for a perfectly flat surface is θ_0, then the value for a real surface, θ, can be estimated from

$$\cos\theta = R_w \cos\theta_0 \qquad (3.2)$$

For wetting surfaces, i.e. $\theta<90°$, roughness will decrease the contact angle. On the other hand, for non-wetting surfaces, roughness will actually increase the contact angle. Thus, surface roughness does not change θ across the 90° boundary.

The experimental data, shown in Table 4, provide qualitative support for the relationship between contact angle and surface roughness. The general trend for both oxidized and non-oxidized surfaces is that well-polished surfaces have larger contact angles than polished ones, and the latter are larger than those of non-polished surfaces. Due to the unavailability of surface roughness data, a quantitative analysis is not possible at the present time. However, one conclusion may be drawn: contact angles on surfaces of TiO_2, ZrO_2 and HfO_2 will not be greater than 90° regardless of the surface finish.

3.2 Surface Adsorption

In addition to surface roughness, other factors can influence contact angles. For example, the adsorption of one monolayer of foreign species can alter the apparent surface tension. This effect can be examined in terms of the spreading pressure,[4,5] π_{sw} , which is defined by

$$\pi_{sw} = \sigma_s - \sigma_{s,a}$$

It is the difference in the surface tension of the surface without and with an adsorbed monolayer, σ_s and $\sigma_{s,a}$, respectively.

The contact angle dependence must, therefore, include the spreading pressure[4,5] term such that

$$\cos\theta_a = \frac{\sigma_s - \sigma_{ws} - \pi_{ws}}{\sigma_w} \qquad (3.3a)$$

$$= 2\frac{W_{a(sw)}}{W_{c(w)}} - \frac{2\pi_{sw}}{W_{c(w)}} - 1 \qquad (3.3b)$$

When $\pi_{sw} > 0$, adsorption will increase the contact angle, and when $\pi_{sw} < 0$, the reverse is true.

In the case of the TiO_2 surface, Figures 7(d) shows a contact angle of 30.7° for a freshly oxidized surface (as retrieved from the oxidation reactor). However, when the contact angle was measured 18 hours later, the angle increased to 65°, as shown in Figure 7(c). The spreading pressure due to the adsorption of water can be estimated by combing Eqs. 1.1 and 3.3a,

$$\pi_{sw}=2\sigma_w(\cos\theta-\cos\theta_a)=0.87\sigma_w$$

where σ_w is the surface tension of water. This gives an estimate for the spreading pressure.

3.3 Reliability of Contact Angle Measurement

Contact angle measurements were conducted on essentially static systems in which the water drop was allowed to come to its final equilibrium value under controlled conditions. When equilibrium is not attained, contact angles will show hysteresis, depending on whether the liquid is advancing across a fresh surface or receding from an already wetted one.

Another factor influencing the measurements is the evaporation of the water drops. For smaller sessile drops (of the order of 0.5mm), the observed initial decrease

in the contact angles is due to evaporation, i.e., the measured contact angles represent receding values because of the retraction of the drop. To minimize the effect of evaporation, the sessile drop sizes used in this work were between 1~2mm. Surface contamination also plays a role in contact angle measurements. The AUGER/ESCA data showed the presence of C and Ar as contaminants. These elements in some molecular forms on the surface may have an effect on the measurement results.

4. PERSPECTIVE AND SUMMARY

The restrictive condition for non-wetting and, hence, waterproofed surfaces implies that most oxide surfaces will not provide waterproofing. Generally, contact angles of H_2O on metal oxides are less than 90°. In order to obtain cases where θ >90, the adhesive energy between water and the oxide surface must be less than half of the cohesive energy of water.

Consider the case of hydroxyl groups attached to a metal oxide surface. Water molecules will interact with these hydroxyls just as water molecules interact with each other. There will be minimal tension on the interface between layers of hydroxyls and water because of their cohesion. Neglecting the interface energy, the work of adhesion $W_{a(ws)}$ for separating the water layer from hydroxyl/surface layer is just equal to $\sigma_w + \sigma_s$, where σ_s is the surface tension of the oxide surface containing hydroxyl groups. Since $W_{c(w)}$ is equal to double the water surface tension, σ_w, the condition $W_{a(ws)} > 0.5W_{c(w)}$ should exist for metal oxide surfaces. Based on the Eq (1.3), this implies that $\cos\theta$ is greater than 0, or θ <90°.

By introducing strongly polarizable heavy metal ions onto the surface of glass, Sonders, et al.[13] observed temporary changes in the hygroscopicity of the surface. They concluded that due to the polarization of the surface ions by the interior Coulombic forces, the repelled electrons counteract the effect of positive excess charge. So the ions became neutral towards the exterior and lost the property to

attract water molecules. Their experimental results showed an increase in the contact angle on the glass to 70° through the introduction of strongly polarizable heavy metal ions. Although this method is not satisfactory for the water-proofing objective, it shows that reducing the attractive interaction between the surface and water is a possible direction to pursue.

Water molecules are polar, each containing a dipole moment of 1.9 Debye units[†]. They can attract surface elements through various types of interactions, primarily through van der Waals forces[5] due to dipole-dipole, dipole-induced dipole, and London dispersion interaction. Conceivably, by minimizing the van der Waals interactions, it is possible to achieve higher contact angles. Since the London dispersion interaction is universal, only other two interactions due to dipole and induced dipole can possibly be absent for some types of materials. These materials can be covalently bonded, and have a small dielectric constant. In addition, the surface of such material must also be shielded by a specially designed layer so that the unsaturated bonds on the fractured surface do not interact with water.

In summary, we have studied the wetting behavior of three type of metal oxide surfaces. These surfaces were formed directly on metal surfaces by oxidation reactions. Simple contact angle measurements on these surfaces revealed that the contact angles were less than 90°. Thus, such oxide surfaces will not provide the needed water-proofing. Various factors affecting the surface contact angles were analyzed based on thermodynamic considerations.

[†] 1 Debye units=3.336×10^{-30} C•m

REFERENCES

1. Schomburg, C., Dotts T.L., and Tillian, DJ, "Moisture Adsorption Characteristics of the Orbiter Thermal Protection System and Methods Used to Prevent Water Ingestion." Presented at the Intersociety Conference on Environmental Systems, July 11-15, 1983. SAE paper #831117

2. Tripp, C.P. and Hair M.L., Langmuir, **7**, 923 (1991).

3. Fisher, R.M., and Dalton, P,"Hygroscopic Characteristic of Space Shuttle Tiles," NASA Contactor Report 177475, December, 1987.

4. Shaw, D.J., "Introduction to Colloid and Surface Science," Butterworths, Boston, 1980.

5. Myeers, D., "Surfaces, Interfaces and Colloids-Principles and Applications," VCH Publishers, Inc, New York, 1991.

6. Henrich, V. E. And Cox, P.A.. "The Surface Science of Metal Oxides," Cambridge University Press, New York, 1994.

7. Miguel A., Blesa, P. J., Morando, A. and Regazzoni, E., Chemical Dissolution of Metal Oxides, CRC Press, Boca Raton, 1993, p131.

8. Henrich, V. E., Prog. Surf. Sci., **14**, 175(1983).

9. Henrich, V. E., in Surface and Interfaces of Ceramic Materials, Dufour, L. C., Monty, C., and Petot-Evans, G., (Eds) NATO ASI Series, Vol. E73, Kluwer, Dordrecht, 1989,1.

10. Kawai, A., and Nagata, H., Jpn. J. Appl. Phys. **33**, 1283 (1994).

11. Wenzel, R. N., Ind. Eng. Chem., **28**, 988(1936).

12. Wenzel, R. N., J. Phys. Colloid Chem., **53**, 1466(1949).

13. Sonders, L. R., Enright, D.P. and Weyl W.A., J. Appl. Phys. **21**, 338 (1950).

FIGURES

Fig. 1. A schematic drawing of a cross-section of thermal insulation tiles, indicating the pores formed by silica fibers.

Fig. 2. Liquid movement in side a capillary, (a) non-equilibrium, (b) equilibrium

Fig. 3. The wettability diagram

Fig. 4. Optical micrographs of (a)A well polished Ti surface, (b) after etching. The insert is the as-received sample surface.

Fig. 5. Schematic diagram of experimental setup for sessile drop contact angle measurement.

Fig. 6. Optical micrographs of sessile drops on (a)well-polished Ti metal surface (b) on surface of as-received Ti sample.

Fig. 7. Optical micrographs of sessile drops on TiO_2 surface formed on well-polished surface by thermal treatment at (a) 280°C (b) 200°C and (c)300°C and (d) 300°C measured immediately after oxidation.

Fig. 8. Optical micrographs of Ti foil surface (a) before and (b)after polishing

Fig. 9. Optical micrographs of sessile drops on surfaces of (a) Ti as-received; (b) TiO_2 form by thermal treatment of Ti at 750° in room air; (c) polished Ti ; and (d) TiO_2 formed by thermal treatment of polished Ti at 750° in room air.

Fig. 10. Optical micrographs of Hf foil surface (a) before and (b)after polishing

Fig. 11. Optical micrographs of Zr foil surface (a) before and (b)after polishing

Fig. 12. Auger spectra of the surface of TiO_2 formed on well-polished foil by thermal oxidation at 300°C

Fig. 13. ESCA peak of thermal oxidized Ti surface for binding energy (BE) of $Ti(2p_{3/2})$ at various stages of ion sputtering.

Fig. 14. XRD spectrum for thermal oxidized Zr surface.

TABLES

Table 1. Specifications of metal foils.

Sample	Source	Purity (%)	Annealing[+]
Ti	JM*	99.7	No
Zr	ESPI*	99.99	Yes
Hf	JM	99.5	Yes

*JM=Johnson and Mathey; ESPI=Electronic Space Product International.

[+]Annealing was done by the supplier in pure argon gas just below the melting point to relieve stress.

Table 2. Surface polishing steps in oxide surface preparation

Steps	1	2	3	4	5	6
Polishing Paper	420 Grit SiC	600 Grit SiC	5μm Diamond	0.3μm Alumina	0.05μm Alumina	3μm Diamond
Polishing time	~2 min	~2 min	~2 min	~2 min	~2 min	~5 min

Table 3. Conditions for metal oxidation

	I	II	III	IV
T_{max} (C)	300	280	200	750
Δt atT_{max} (min)	10	10	10	30
O_2 (c.c./min)	80	80	80	room Air
Ar (c.c./min)	40	40	40	room Air

Table 4. Contact angles on metal and oxide surfaces (degree)

A. Ti foil

non-polished(Fig 8a)		polished (Fig 8b)		well-polished (Fig 4)			
				Oxidized by			
Non-Oxidized	Oxidized by IV*	Non-Oxidized	Oxidized by IV*	Non-Oxidized	I*	II*	III*
52	16	59	28	86.9	65	63	62

* Roman numbers refer to conditions listed in Table 3.

B. Hf foil

non-polished(Fig 10a)		polished (Fig 10b)	
Non-Oxidized	Oxidized by IV*	Non-Oxidized	Oxidized by IV*
71	15	75	23

* Roman numbers refer to conditions listed in Table 3.

C. Zr foil

non-polished(Fig 11a)		polished (Fig 11b)	
Non-Oxidized	Oxidized by IV*	Non-Oxidized	Oxidized by IV*
68	25	73	47

* Roman numbers refer to conditions listed in Table 3.

Figure 1.

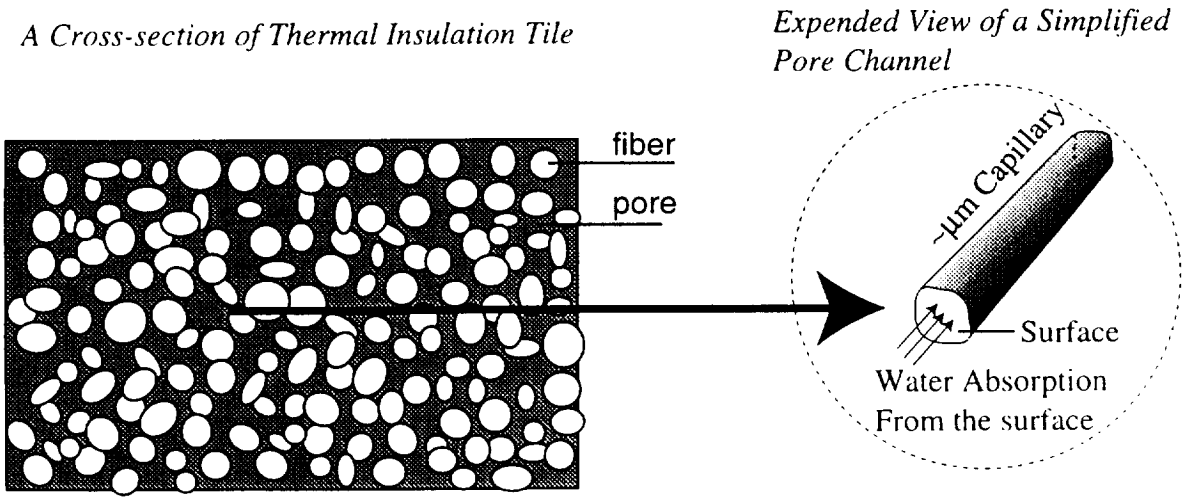

Figure 2.

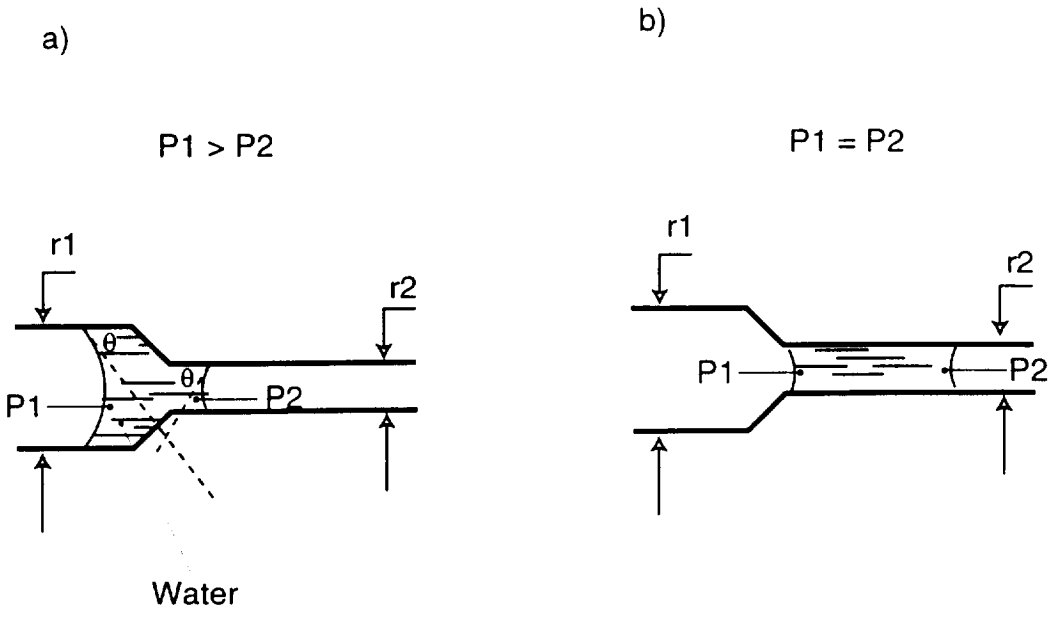

Figure 3.

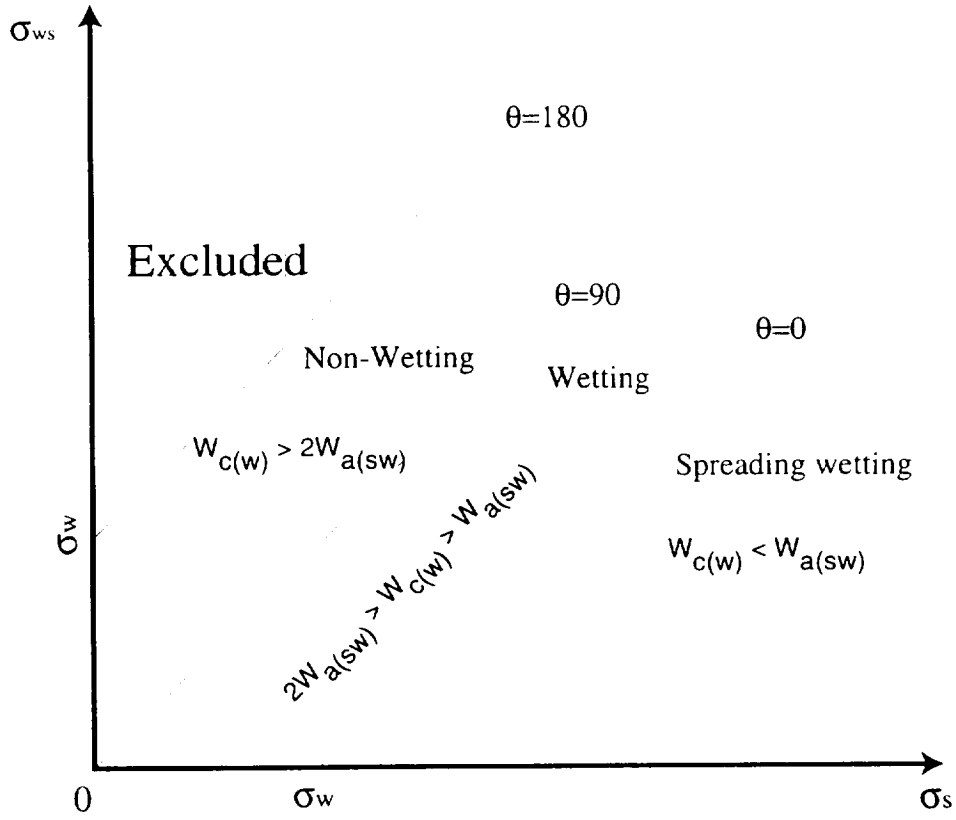
σws
θ=180
Excluded
θ=90
θ=0
Non-Wetting
Wetting
Wc(w) > 2Wa(sw)
Spreading wetting
2Wa(sw) > Wc(w) > Wa(sw)
Wc(w) < Wa(sw)
σw
0
σw
σs

Fig. 4a

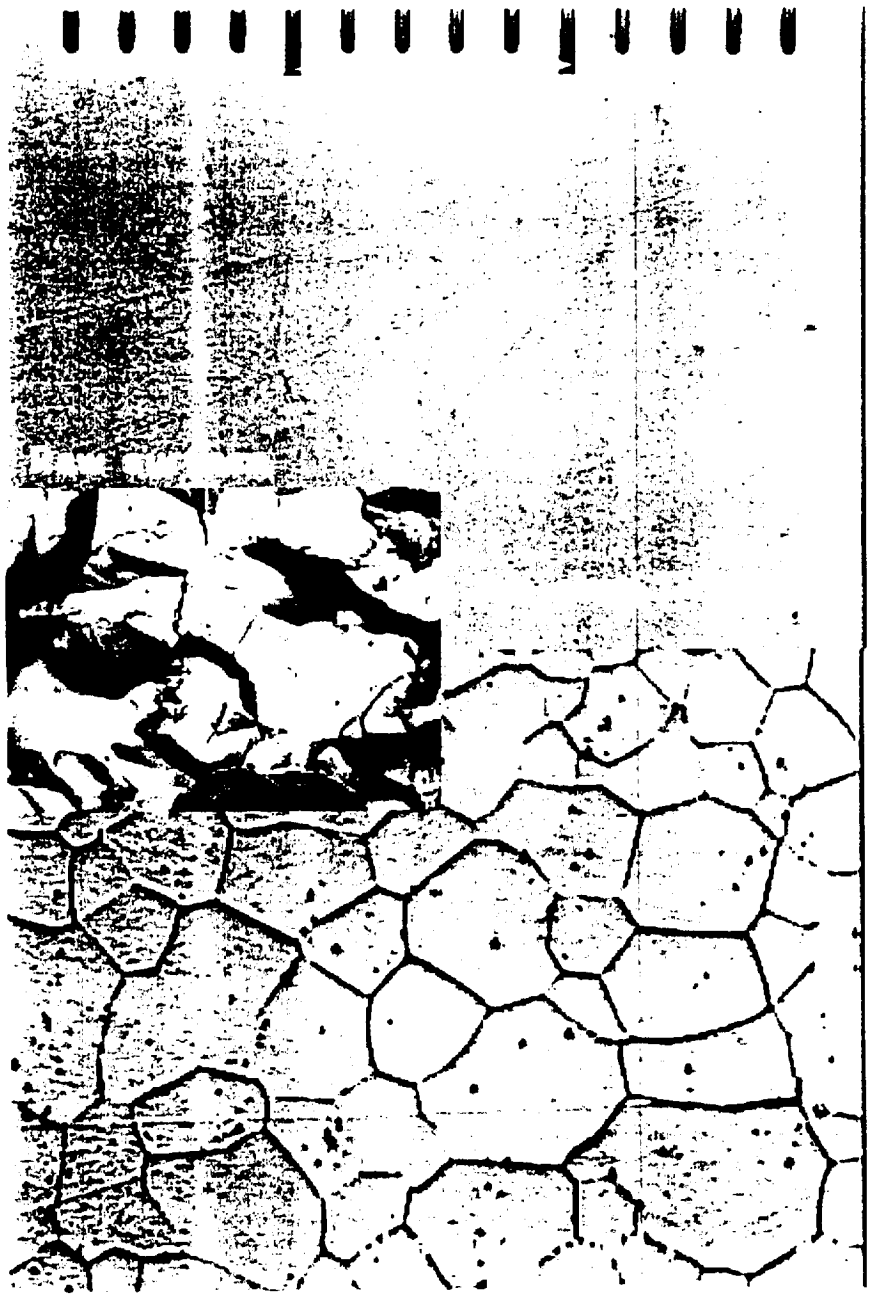

Fig. 4b

Figure 5

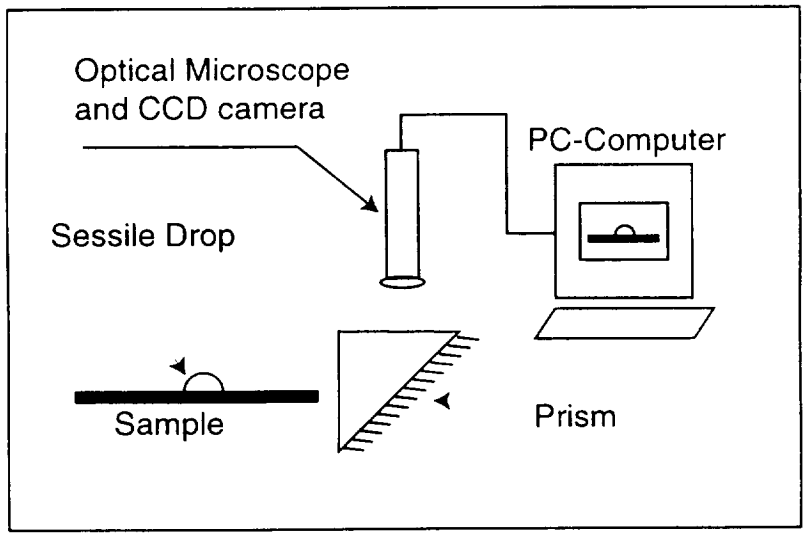
Optical Microscope
and CCD camera
PC-Computer
Sessile Drop
Sample
Prism

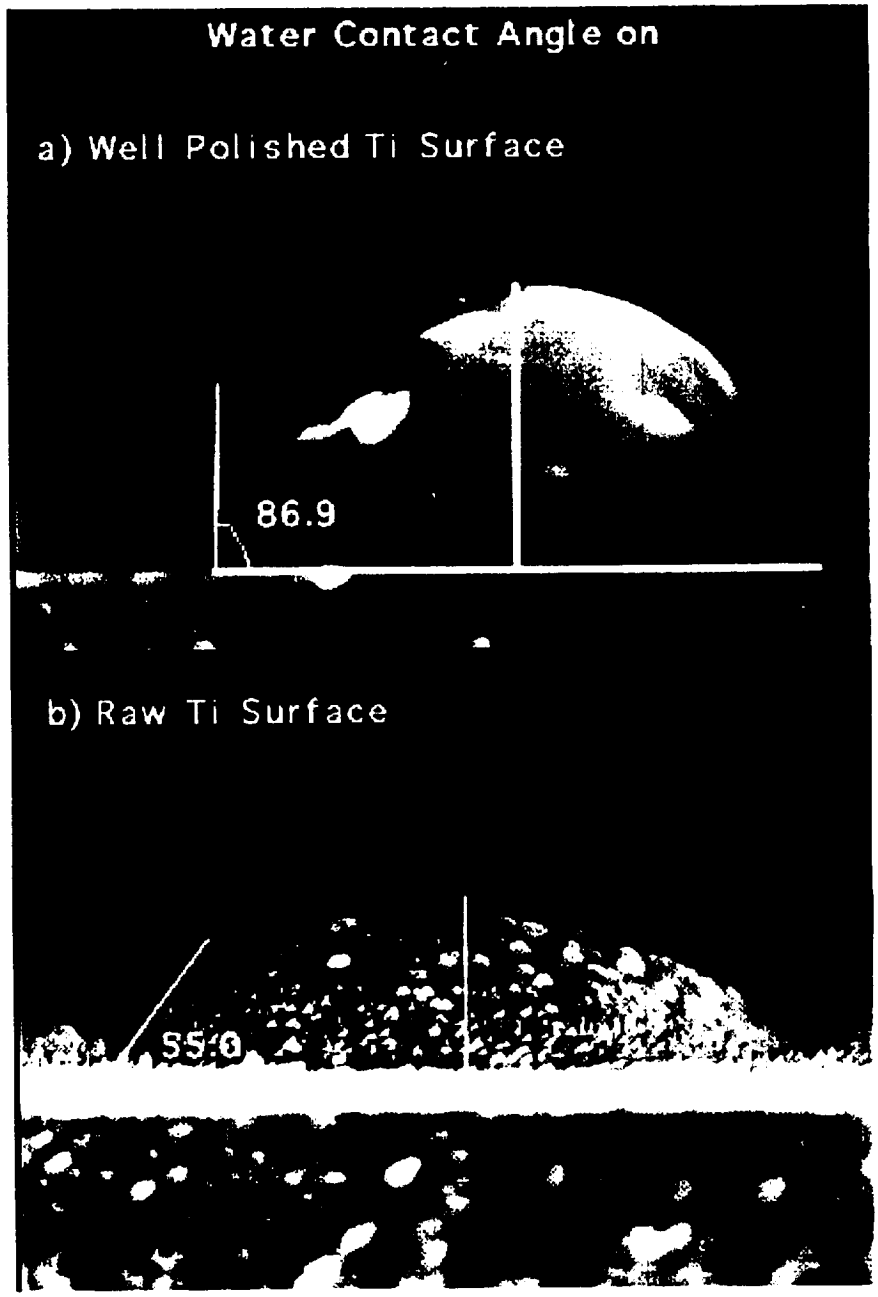
Water Contact Angle on
a) Well Polished Ti Surface
86.9
b) Raw Ti Surface
55.0

Fig. 6a

Fig. 6b

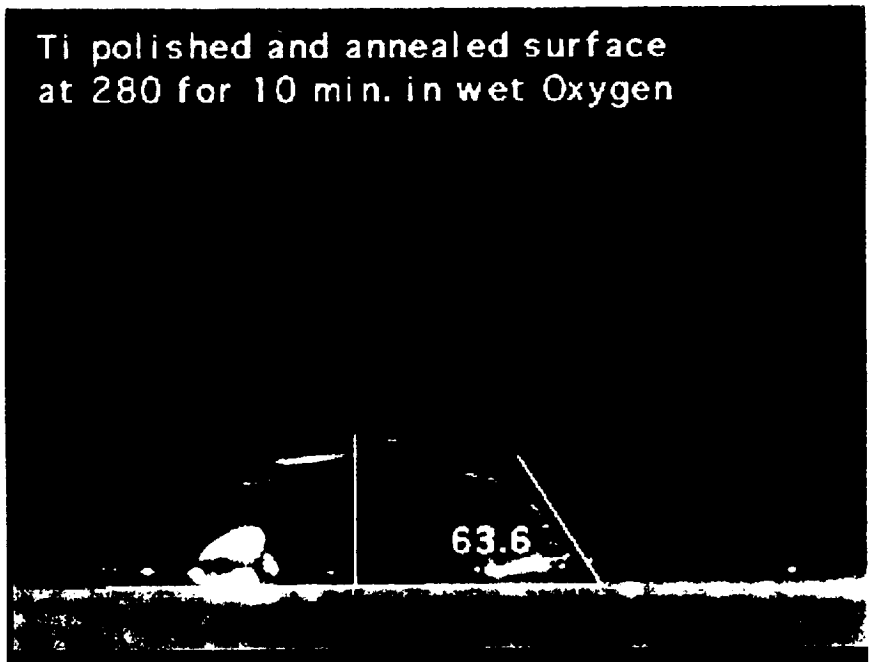
Ti polished and annealed surface
at 280 for 10 min. in wet Oxygen
63.6

Fig. 7a

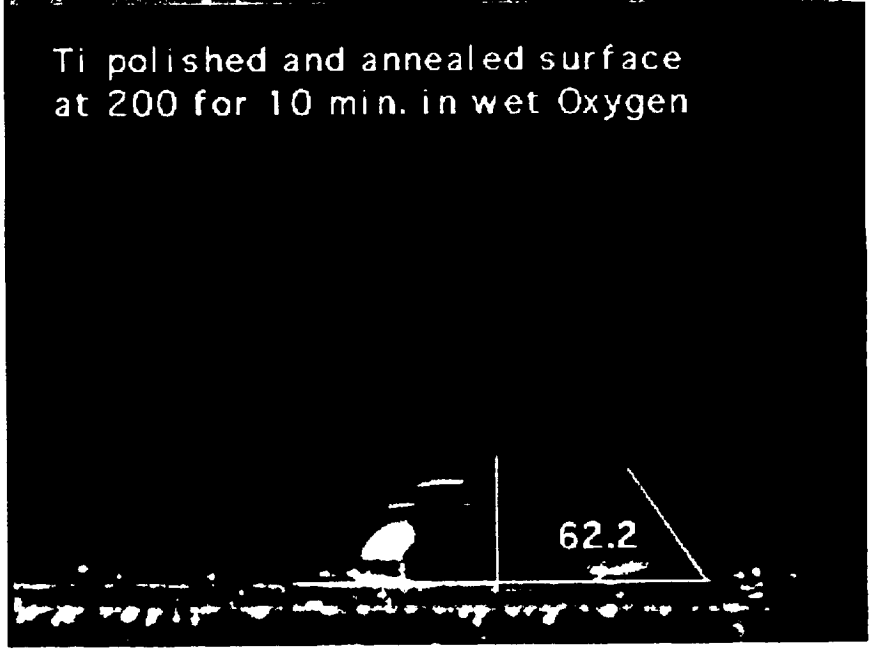
Ti polished and annealed surface
at 200 for 10 min. in wet Oxygen
62.2

Fig. 7b

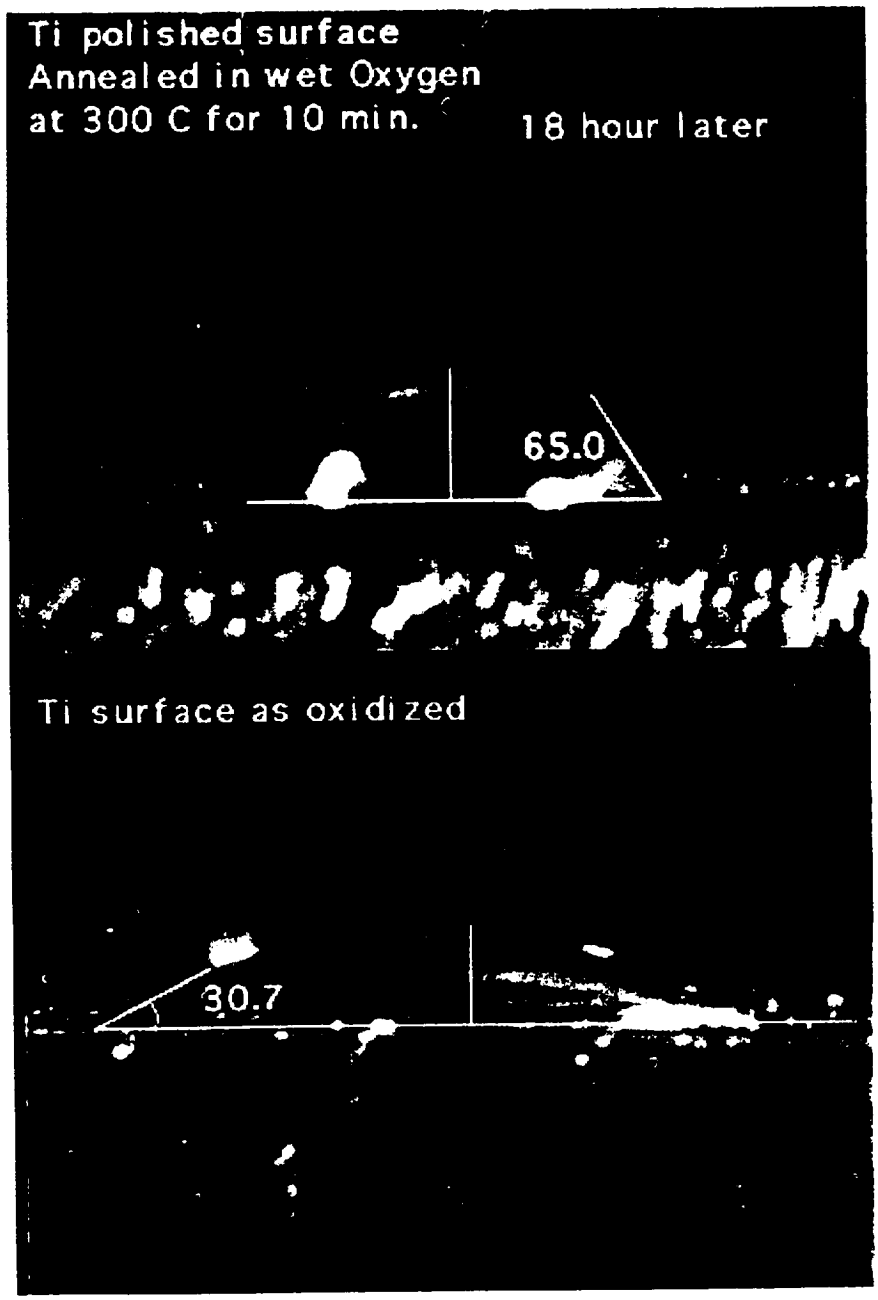
Ti polished surface
Annealed in wet Oxygen
at 300 C for 10 min.
18 hour later
65.0
Ti surface as oxidized
30.7

Fig. 7c

Fig. 7d

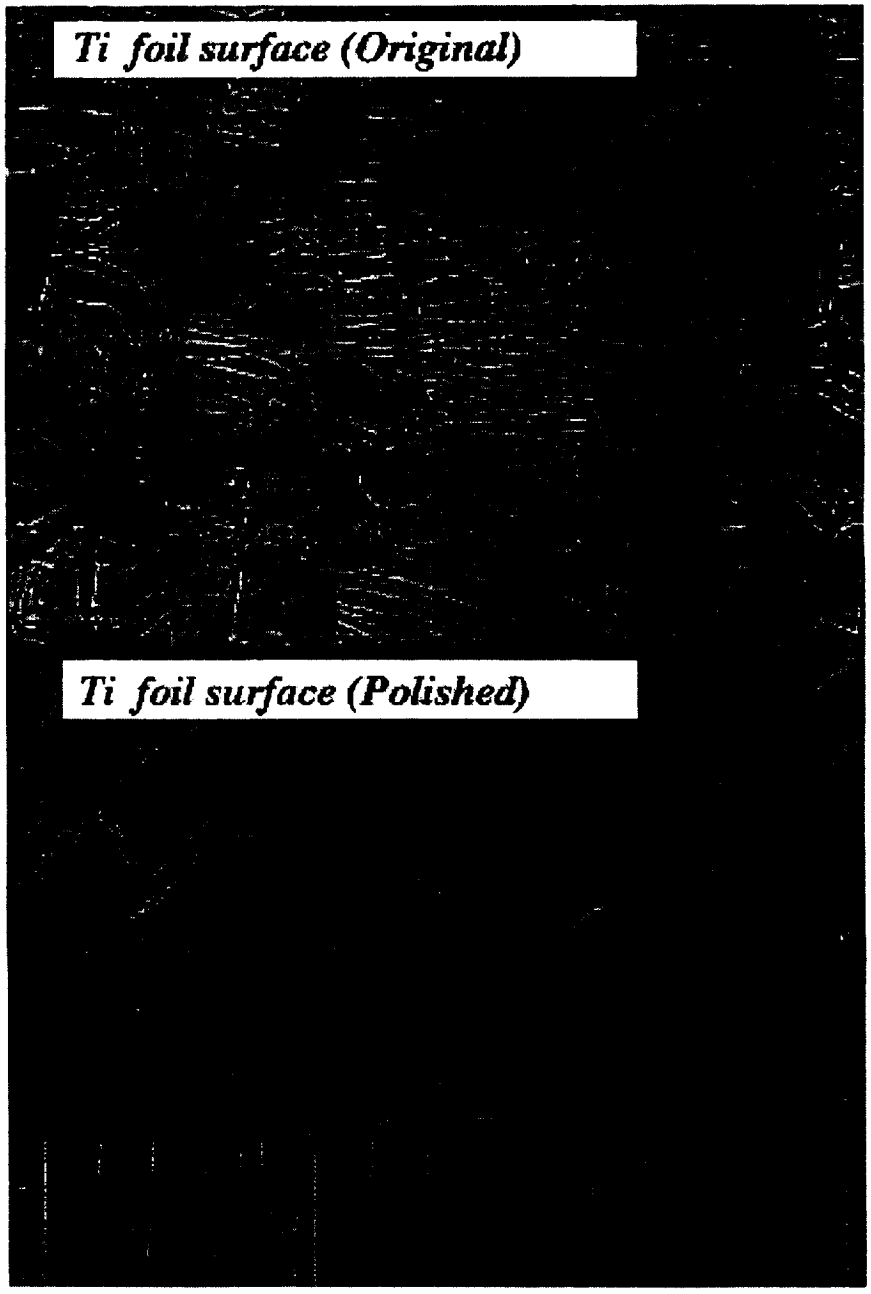

Fig. 8a

Fig. 8b

Fig. 9a

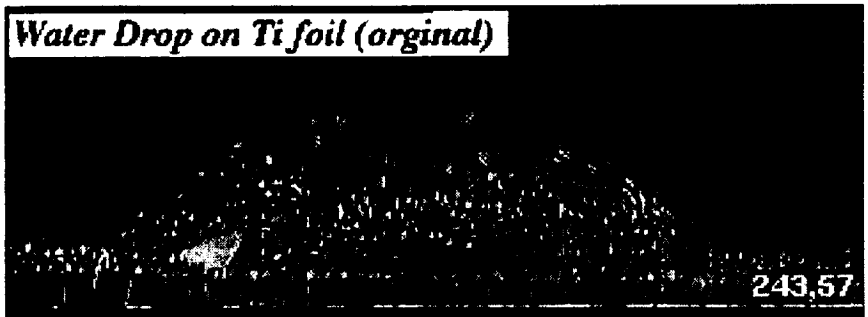

Fig. 9b

Fig. 9c

Fig. 9d

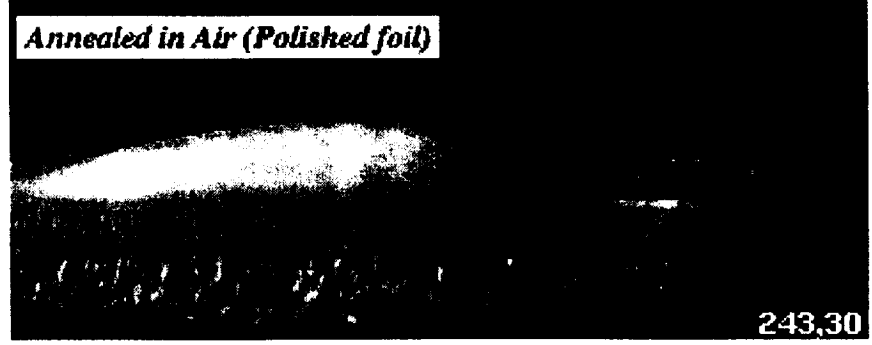

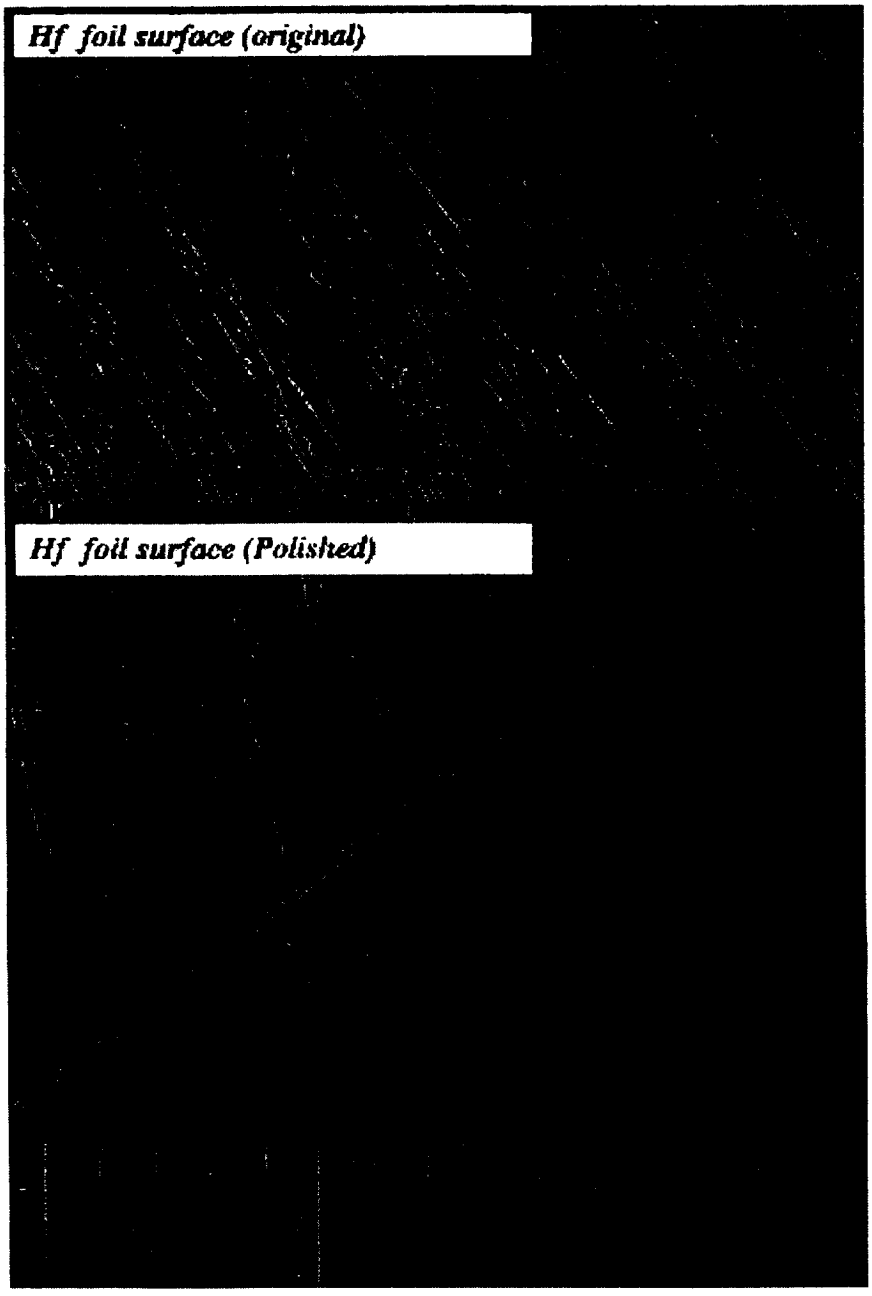

Fig. 10a

Fig. 10b

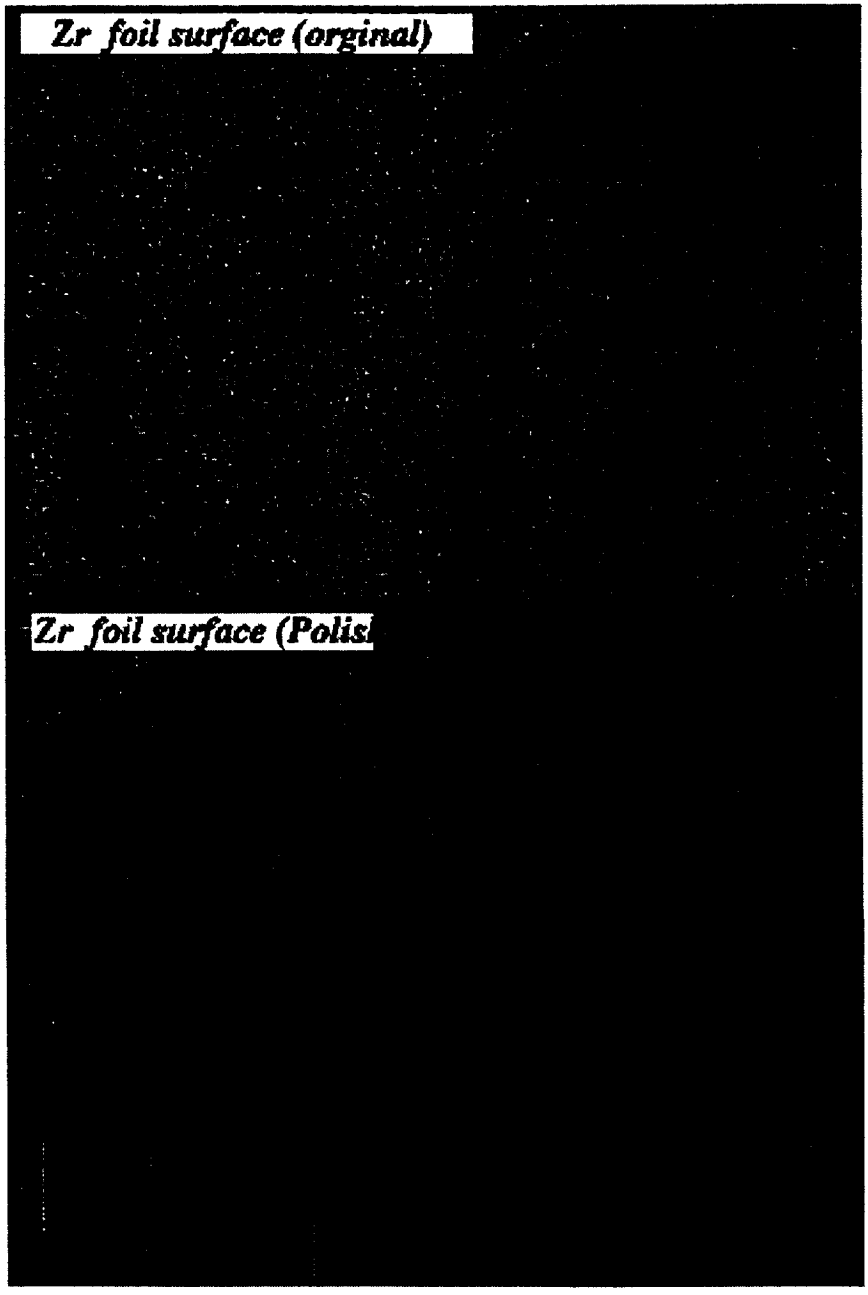

Fig. 11a

Fig. 11b

Fig. 12

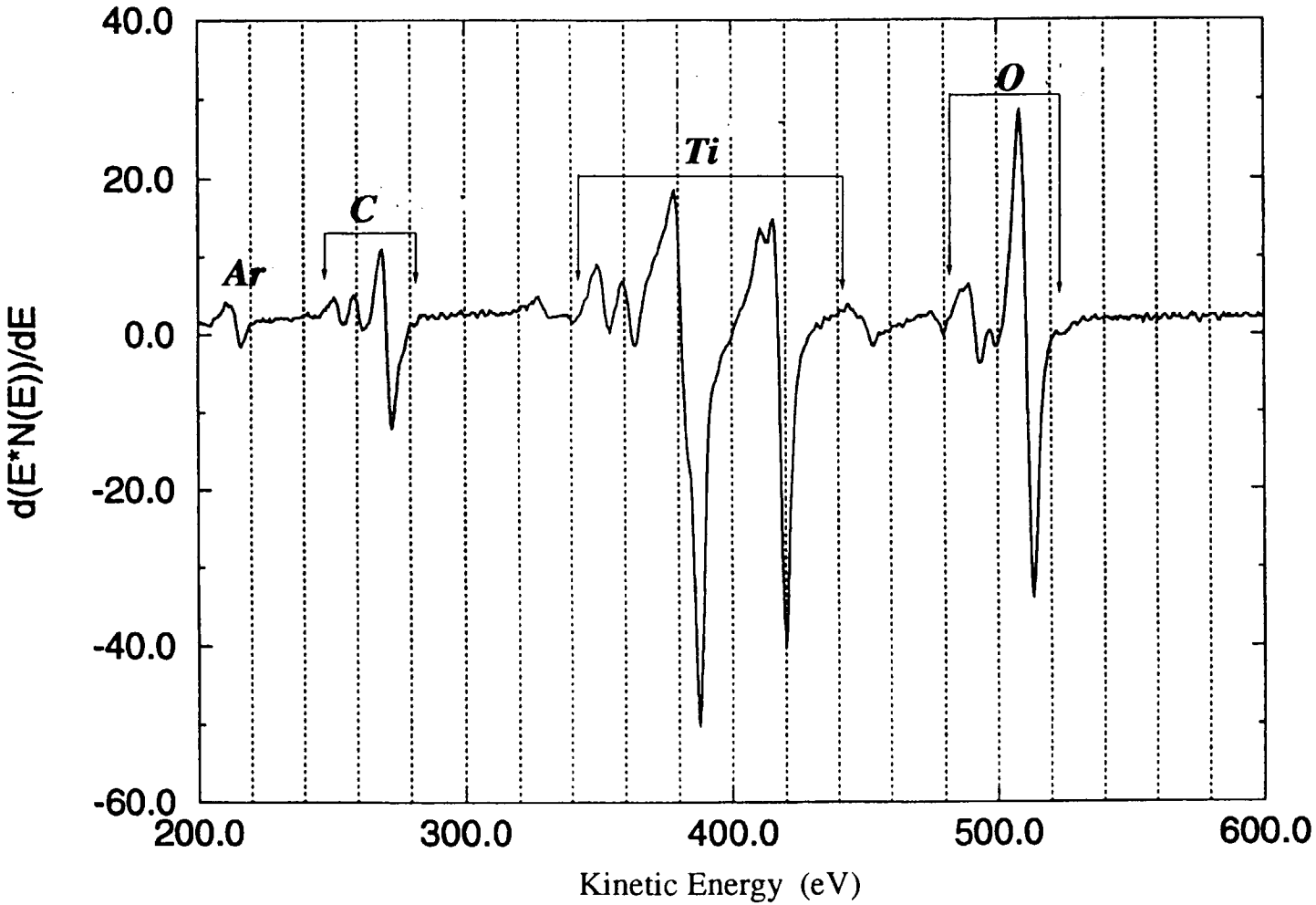
40.0
20.0
0.0
-20.0
-40.0
-60.0
d(E*N(E))/dE
Ar
C
Ti
O
200.0
300.0
400.0
500.0
600.0
Kinetic Energy (eV)

Fig. 13

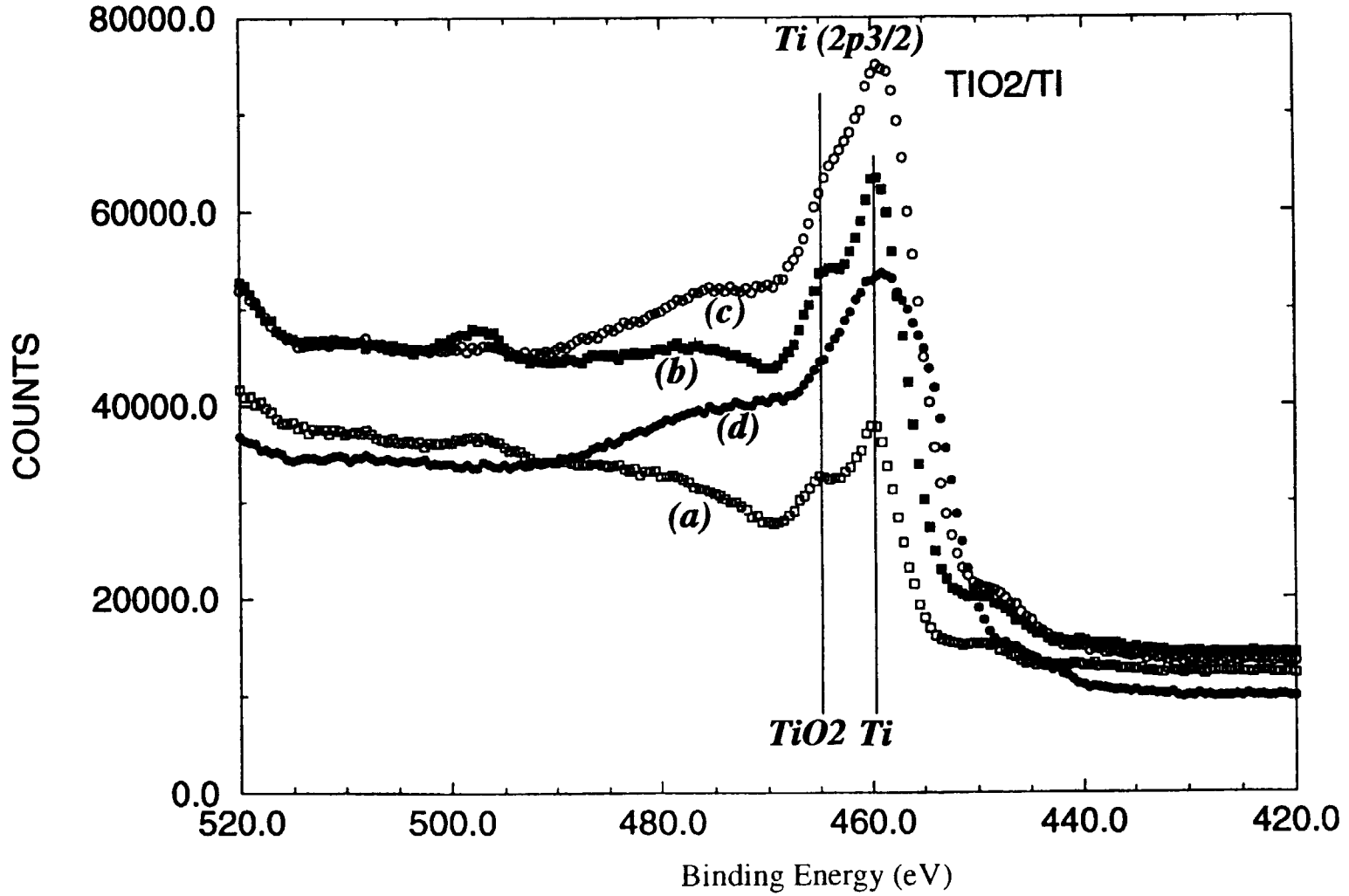
80000.0
60000.0
40000.0
20000.0
0.0
COUNTS
Ti (2p3/2)
TIO2/TI
(c)
(b)
(d)
(a)
TiO2 Ti
520.0
500.0
480.0
460.0
440.0
420.0
Binding Energy (eV)

Fig. 14

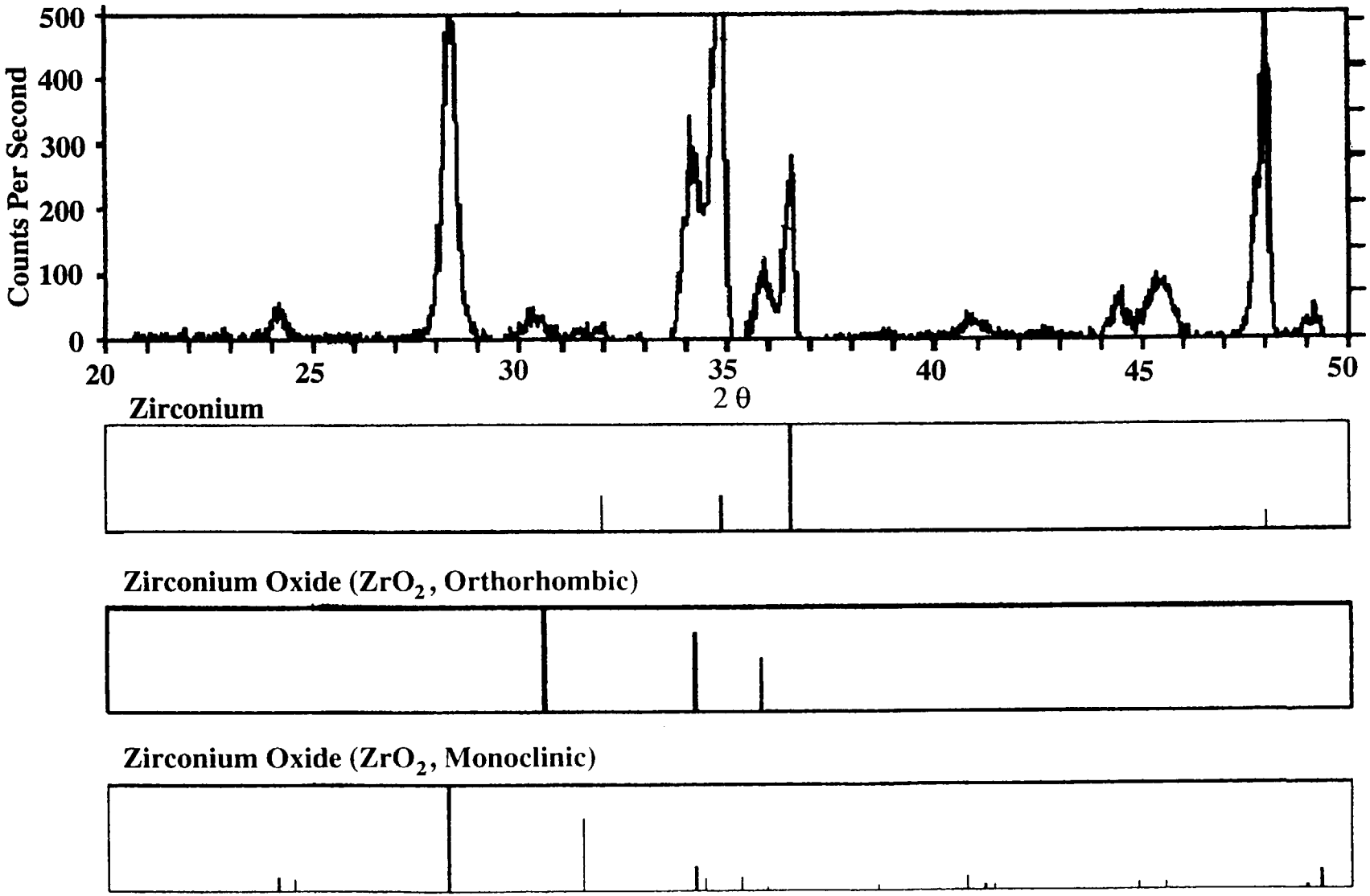
Counts Per Second
500
400
300
200
100
0
20
25
30
35
40
45
50
2 θ
Zirconium
Zirconium Oxide (ZrO_2, Orthorhombic)
Zirconium Oxide (ZrO_2, Monoclinic)

NASA	Report Documentation Page	
1. Report Number	2. Government Accession No.	3. Recipient's Catalog No.
4. Title and Subtitle Thermal Stability of Surface Coatings on Thermal Protection System (TPS): Measurement of the Surface Properties of High Temperature Oxides		5. Report Date Nov. 14, 1995 6. Performing Organization Code
7. Author(s) Aiguo Feng, Zuhair Munir, Ben McCoy, Domenick Cagliostro		8. Performing Organization Report No. 10. Work Unit No.
9. Performing Organization Name and Address Department of Chemical Engineering and Materials Science University of California, Davis, CA 95616		11. Contract or Grant No. NCC2-5090 13. Type of Report and Period Covered
12. Sponsoring Agency Name and Address National Aeronautics and Space Administration Washington, D.C. 20546		14. Sponsoring Agency Code
15. Supplementary Notes Point of Contact: D.E. Cagliostro 223-4, Thermal Protection Branch, NASA Ames Research Center Moffett Field, CA 94035		

16. Abstract

We have studied the wetting behavior of three metal oxide surfaces. These surfaces were formed directly on metals by oxidation reactions. Simple measurements for water on these surfaces revealed that the contact angles were less than 90°. Thus, such oxide surfaces will not provide the needed waterproofing. Various factors affecting the surface contact angles were analyzed based on thermodynamic considerations.

17. Key Words (Suggested by Author(s))	18. Distribution Statement		
Silica; waterproofing; thermal insulation; hydrophobic and hydrophilic; oxides; contact angle; wettability; surface energy or tension			
19. Security Classif. (of this report) Unclass	20. Security Classif. (of this page) Unclass	21. No. of Pages 31	22. Price